ACS OMEGA

Open Access

http://pubs.acs.org/journal/acsodf

Article

High-Yield Preparation and Properties of Phenolic Resin-Based Carbon Microspheres

Jian Shao, Junzong Feng,* Yonggang Jiang, Liangjun Li, Yijie Hu, and Jian Feng*

Cite This: *ACS Omega* 2024, 9, 43583−43592

Read Online

ACCESS | Metrics & More | Article Recommendations

ABSTRACT: This study aims to enhance the production efficiency of carbon microspheres (CS) and expand their potential applications. To this end, resorcinol-formaldehyde microspheres (RFS) were prepared in high yield through the modified Stöber method, utilizing resorcinol and formaldehyde as carbon sources, ammonia as a catalyst, and sodium dodecyl benzenesulfonate (SDBS) as a soft template. The resulting RFS were then carbonized to obtain high yield CS. This study examined the impact of key factors, namely, the concentration of resorcinol, ammonia, and the SDBS concentration, along with the temperature of carbonization, upon the properties of the resulting CS, which were observed with regard to microscopic morphology, average particle size, homogeneity, and yield. The findings demonstrated that the proclivity of RFS to agglomerate with one another at high carbon source concentrations was markedly diminished, while the yield of CS was notably enhanced through the introduction of the anionic surfactant SDBS. The particle size of RFS can be modified within the range 200−1000 nm by adjusting the resorcinol and ammonia concentration. The prepared RFS exhibited a regular spherical morphology and a smooth surface. Furthermore, the CS displayed a uniform spherical morphology following high-temperature carbonization, with no agglomeration or cross-linking observed between adjacent particles. It was observed that the yield of RFS reached a maximum of 93.2 g/L when the resorcinol concentration was 0.7 mol/L. Following carbonization at 800 °C, the yield of CS was found to be 41.9 g/L, with a diameter of 770 nm and good monodispersity.

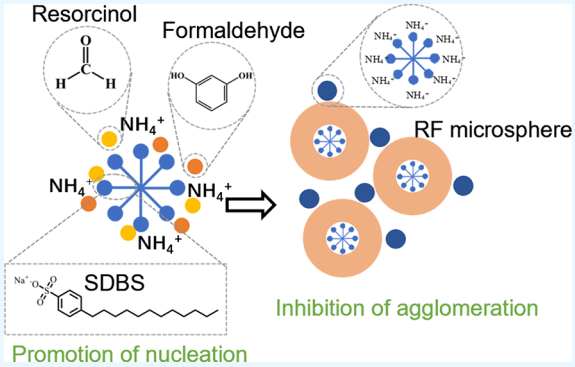

1. INTRODUCTION

With good dispersion and fluidity, high packing density, large specific surface area, short ion diffusion distance, and rich pore structure, carbon microspheres (CS) show promising applications in the fields of catalysis, adsorption, drug delivery, energy storage, and energy conversion.[1−6] For example, CS with high specific surface area can be used as electrode materials for supercapacitors with better electrostatic adsorption and electrochemical performance;[7−12] the microporous structure in CS can be used for CO_2 adsorption, this physical adsorption process based on porous solid adsorbent has a lower cost and stronger regeneration capacity compared with the currently used chemisorption;[13,14] CS are also an excellent electrocatalyst carrier material.[15−18] The high surface area and the rich porous structure can effectively load highly dispersed metal nanoparticles for catalysis, and the high electrical conductivity makes the CS have relatively high charge transfer efficiency.[18−21]

So far, several methods have been developed to synthesize CS, including chemical vapor deposition, arc discharge, spray pyrolysis, hydrothermal method, and the modified Stöber method.[22−26] Compared with other synthesis methods, the extension of the Stöber method uses polymers such as phenolic resins as precursors, with lower synthesis temperature and pressure, higher safety, and lower cost, and has unique advantages in industrial production.[27−30]

The extension of the Stöber method was proposed by Liu et al. in 2011, which has a similar mechanism to the conventional stöber method for the synthesis of SiO_2 microspheres, using ammonia as a catalyst in a mixed solution of water and alcohol to polymerize phenol and formaldehyde to obtain phenolic resin spheres.[31] Since then, many researchers prepared a variety of pore structures and functionally rich nanocarbon microspheres by the extension of the Stöber method, further demonstrating their promising applications.[32−35] However, to prevent the mutual agglomeration of resorcinol−formaldehyde microspheres (RFS) during the polymerization process, very low precursor concentrations were often adopted in most of the papers, resulting in low yields of phenolic-based CS (generally less than 20 g/L) and high costs. Xu et al.[18]

Received: June 14, 2024
Revised: August 28, 2024
Accepted: September 3, 2024
Published: October 16, 2024

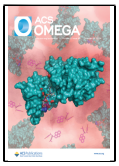

synthesized RFS with a diameter of 810 nm using a concentration of resorcinol of only 0.05 mol/L. Zhao et al.[34] showed that the polymerization products underwent a large degree of agglomeration at a precursor resorcinol concentration of 0.175 mol/L, and no dispersed microspheres could be obtained. In order to obtain higher yields, Li et al.[36] used low-reactivity phenol as the precursor, cetyltrimethylammonium bromide (CTAB) as the stabilizer, and 2,2-bis-(hydroxymethyl)-2,2′,2″-nitrilotriethanol (Bis-tris) as the catalyst. Bis-tris could provide a near-neutral environment and slow down the reaction, and well-dispersed CS were prepared even at high precursor concentrations (0.2 mol/L). However, this method requires a two-step hydrothermal process, and the reaction must be carried out in an autoclave at 200 °C, which is a cumbersome process and requires high equipment requirements. To reduce the tendency of agglomeration during microsphere polymerization at high precursor concentrations, Yu et al. developed a high-yield preparation method for monodisperse phenolic microspheres and CS based on the autocatalytic reaction between phenol derivatives and hexamethylenetetramine.[37] The concentration of precursor m-aminophenol reaches 0.23 mol/L, and the yields of phenolic microspheres and corresponding CS can reach 29.9 and 15.9 g/L, respectively, when the diameter of CS is about 600 nm, but there is still space for further improvement.

In this study, highly yielded RFS and corresponding CS were prepared using resorcinol and formaldehyde as carbon sources, ammonia as the catalyst, and sodium dodecyl benzenesulfonate (SDBS), an anionic surfactant, as a soft template. It was observed that, when the concentration of precursor resorcinol is 0.7 mol/L, monodisperse microspheres can still be prepared, and the yield of RFS is 93.2 g/L. The yield of corresponding carbon spheres is up to 41.9 g/L, with a particle size of only 770 nm. The particle size of carbon spheres can be adjusted within the range 200−800 nm by adjusting the synthesis conditions. The CS produced by high-temperature carbonization exhibited monodispersity and a regular spherical shape of RFS, similar to that of RFS, and displayed a high specific surface area. The method is conducted at lower temperatures and atmospheric pressure without the use of ethanol as a solvent. The synthesis conditions are mild, which are conducive to large-scale and high-efficiency synthesis.

2. RESULTS AND DISCUSSION

2.1. Morphology and Yield Characterization of RFS. A series of experiments were conducted by varying the synthesis parameters in order to analyze the effects of various factors on the morphology, mean particle size, homogeneity, and yield of RFS. The coefficient variation (CV) is used to measure the monodispersity of microsphere particle size, which is calculated as

$$\overline{D_n} = \sum_{i=1}^{N} D_i/N \tag{1}$$

$$\mathrm{CV} = \left[\sum_{i=1}^{N} \frac{(D_i - \overline{D_n})^2}{N}\right]^{1/2} / \overline{D_n} \tag{2}$$

where D_i is the diameter of the RFS (nm), N is the total number of selected RFS, and $\overline{D}_n$ is the average diameter of the selected RFS (nm).

Figure 1 shows the SEM pictures of RFS with and without the addition of SDBS (resorcinol concentration, 0.5 mol/L; formaldehyde concentration, 1.0 mol/L; ammonia concentration, 0.5 mol/L; reaction temperature, 45 °C). It can be seen from the figure that the RFS without the addition of SDBS showed serious agglomeration. The microspheres with a diameter of about 2 μm are connected together and lose their monodisperse state. The RFS with the addition of SDBS still maintains a small particle size and high uniformity, which proves that SDBS plays a very significant inhibitory role in reducing the particle size and the tendency of microsphere agglomeration.

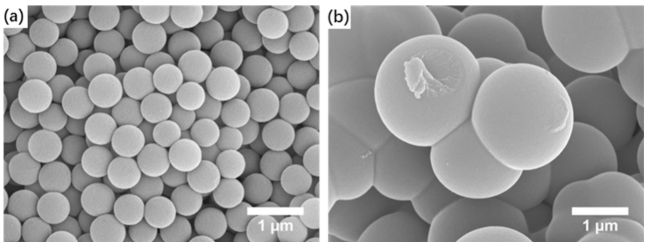

Figure 1. Effects of (a) adding SDBS and (b) not adding SDBS on the microscopic morphology of RFS.

In addition to the anionic surfactant SDBS used in this study, the cationic surfactant CTAB[38] and the nonionic surfactant F127[39] (three block copolymer, PEO−PPO−PEO) can be used as a soft stencil for the preparation of CS. The resorcinol concentration was kept at 0.2 mol/L and the ammonia concentration was 0.2 mol/L in this series of experiments. Figure 2 shows the SEM pictures of the RFS prepared with different surfactants. The figure illustrates that the RFS is uniformly dispersed with the addition of SDBS. However, with the addition of F127, the RFS comprises a multitude of diminutive spheres with a diameter of 100 nm and a few larger spheres with a diameter exceeding 1 μm. This results in a notable decline in monodispersity. After the addition of CTAB, the RFS generate serious mutual agglomeration and lose their spherical shape. It can be seen that the use of SDBS as a templating agent is more favorable to obtain RFS with small particle size and high yield. The rationale behind this phenomenon may be attributed to the ability of the anionic surfactant SDBS to bind with NH_4^+, a process that is facilitated by the electrostatic attraction between the negative charge on SDBS and the positive charge on NH_4^+.[40,41] In contrast, CTAB and F127 have relatively low stability, are difficult to maintain in high concentrations in high precursor solutions, and are prone to agglomeration. This makes it difficult for them to function as soft template agents and interferes with the nucleation and growth processes of RFS.

In this study, a reasonable explanation is proposed to elucidate the mechanism of SDBS in reducing the particle size and the agglomeration of microspheres, as shown in Figure 3. SDBS is an amphiphilic surfactant with hydrophobic alkyl and hydrophilic sulfonic acid groups, which will self-assemble into micelles with the hydrophobic end inward and hydrophilic end outward after dissolving in water. Due to the electrostatic gravitational effect, NH_4^+ in the solution will be arranged in the hydrophilic end of SDBS micelles, while the hydrophilic end of SDBS will undergo organic−organic self-assembly with resorcinol and formaldehyde.[40,41] Resorcinol and formalde-

https://doi.org/10.1021/acsomega.4c05590
ACS Omega 2024, 9, 43583−43592

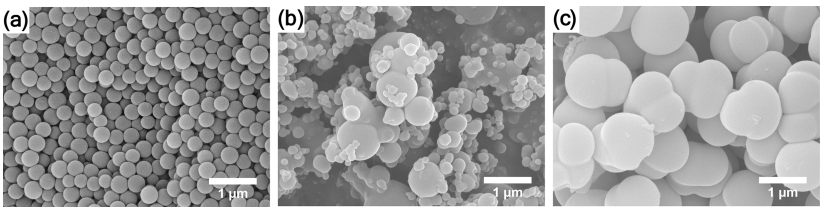

Figure 2. SEM images of RFS prepared with different kinds of surfactants: (a) SDBS, (b) F127, (c) CTAB.

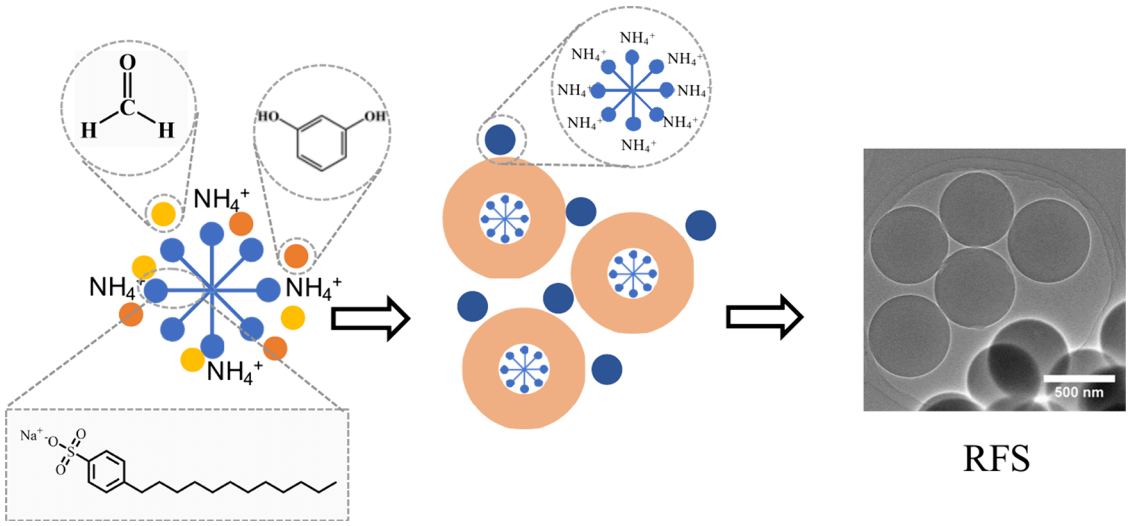

Figure 3. Schematic diagram of RFS synthesis.

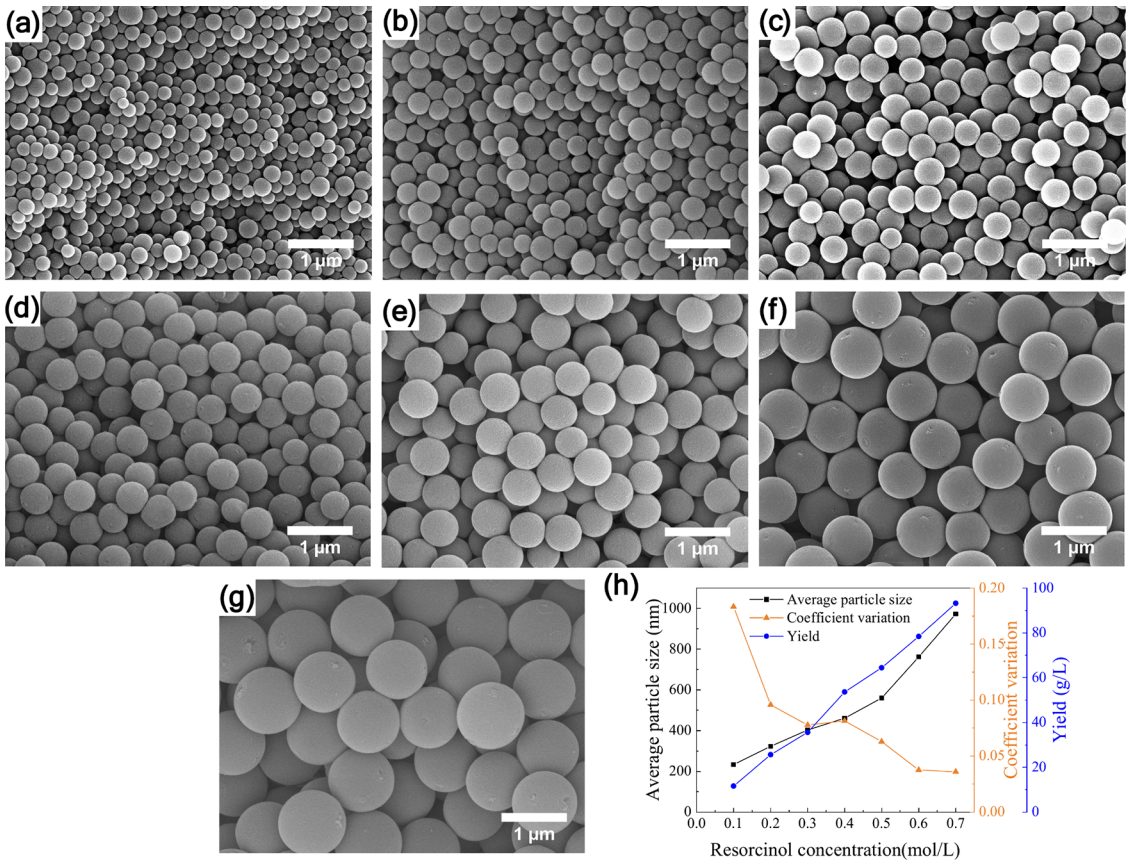

Figure 4. SEM images of RFS prepared with different resorcinol concentrations. (a) 0.1 mol/L, (b) 0.2 mol/L, (c) 0.3 mol/L, (d) 0.4 mol/L, (e) 0.5 mol/L, (f) 0.6 mol/L, and (g) 0.7 mol/L. (h) Mean particle size, coefficient variation, and yield of RFS with resorcinol concentration.

https://doi.org/10.1021/acsomega.4c05590
ACS Omega 2024, 9, 43583−43592

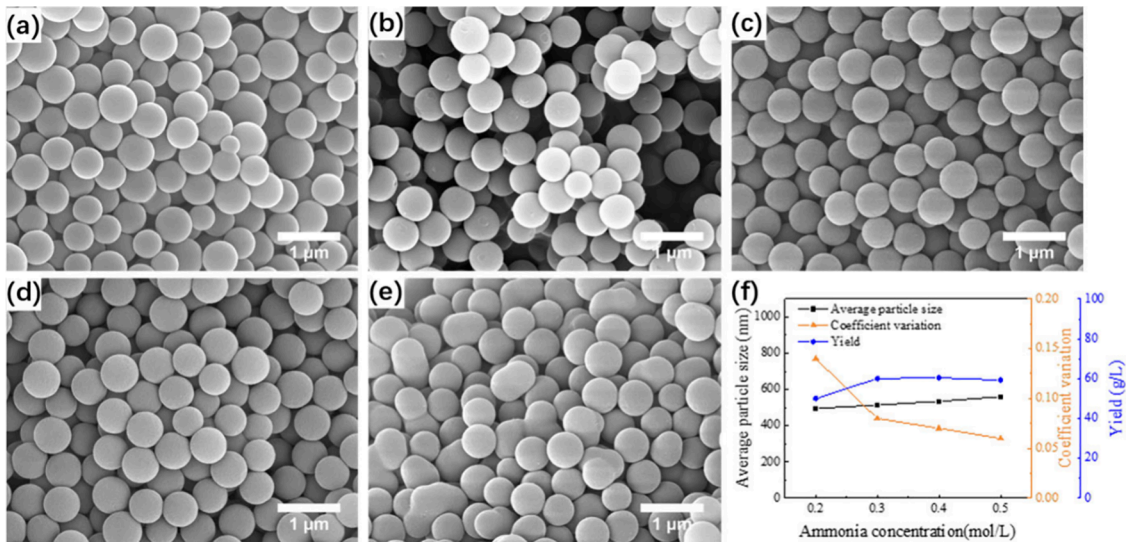

Figure 5. SEM images of RFS prepared with different ammonia concentrations: (a) 0.2 mol/L, (b) 0.3 mol/L, (c) 0.4 mol/L, (d) 0.5 mol/L, and (e) 0.6 mol/L. (f) Mean particle size, coefficient variation, and yield of RFS with ammonia concentration.

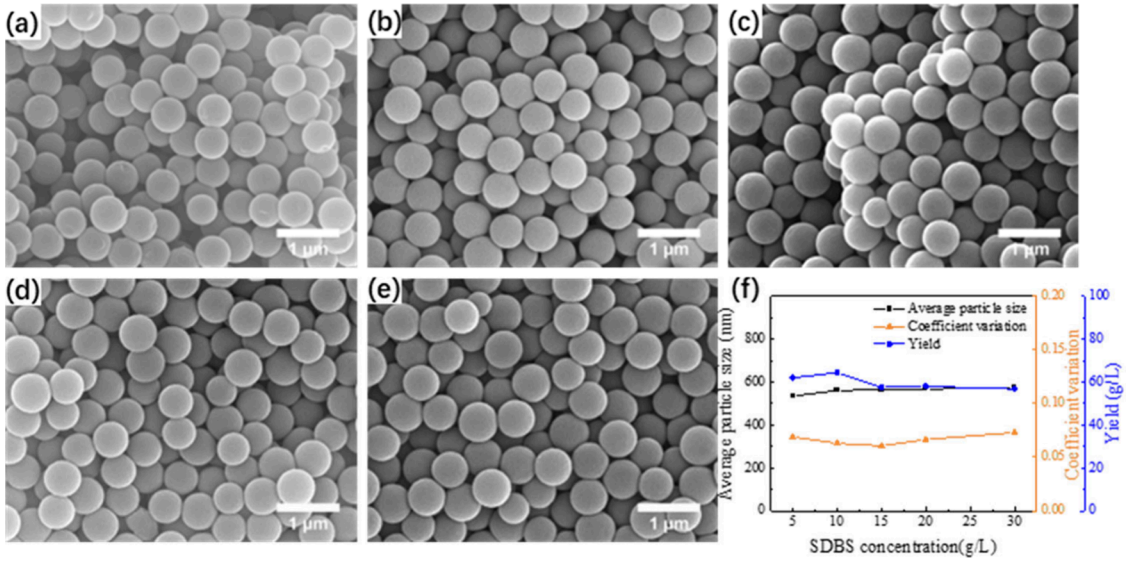

Figure 6. SEM images of RFS prepared with different SDBS concentrations: (a) 5, (b) 10, (c) 15, (d) 20, and (e) 30 g/L. (f) Mean particle size, coefficient variation, and yield of RFS with various SDBS concentrations.

hyde near the hydrophilic end of SDBS micelles will produce various derivatives catalyzed by NH_4^+ and form emulsion droplets wrapped around the micelles on the surface of SDBS micelles driven by the minimum surface energy. In this process SDBS micelles act as a soft templating agent and increase the nucleus formation of the RFS. As the reaction continues, the droplets are increasingly cross-linked and finally solidify to RFS. During the formation of RFS, NH_4^+ will attach to the surface of RFS, which can inhibit microsphere agglomeration to some extent.[31] The higher stability of SDBS micelles bound to NH_4^+ ensured a high concentration of SDBS in solution. The spatial site-blocking effect of the long-chain segments of SDBS disperses the reactants and catalysts, which greatly inhibits agglomeration during RFS growth.

In this study, a series of experiments were conducted to investigate the effects of carbon precursor concentration, catalyst concentration, and SDBS on the microscopic morphology and yield of RFS, which are presented in turn.

Figure 4 shows SEM images of RFS prepared with different resorcinol concentrations and the mean particle size, coefficient variation, and yield of RFS with resorcinol concentration. The molar ratio of ammonia to resorcinol was maintained 1:1, and the molar ratio of resorcinol to SDBS was 17:1 in this series of experiments. It can be seen from the images that each sample has a regular spherical shape. The distribution of spheres with different diameters in Figure 4a and b showed poor particle size uniformity, while the RFS in Figure 4c−g had a narrow particle size distribution and high uniformity.

As shown in Figure 4h, the average particle size and yield of the RFS increase approximately linearly with increasing resorcinol concentration. It is worth noting that monodisperse RFS can be obtained even when the resorcinol concentration is increased to 0.7 mol/L, which indicates that the addition of SDBS significantly reduces the agglomeration tendency of droplets during the polymerization process. At this time, the

https://doi.org/10.1021/acsomega.4c05590
ACS Omega 2024, 9, 43583−43592

average particle size of RFS is only 972 nm, and the yield reaches 93.20 g/L. When the minimum resorcinol concentration is 0.1 mol/L, the coefficient variation of RFS reaches 0.1833, with poor monodispersity. As the concentration of resorcinol increased, the coefficient variation decreases rapidly to a minimum of 0.0360, and the monodispersity of RFS improves significantly. It is speculated that this is because when the precursor concentration is higher, the number of RFS per unit volume in the solution is greater. The greater mutual repulsion between the RFS resulted in a uniform growth rate of the microspheres and ultimately better monodispersity.

Figure 5 shows the SEM images of RFS prepared with different ammonia concentrations and the average particle size, coefficient variation, and yield of RFS with an ammonia concentration. The yield is low when the ammonia concentration is low (0.2 mol/L). The yield of RFS increased to about 60 g/L after the ammonia concentration increased and remained stable. Until the ammonia concentration increases to 0.6 mol/L, RFS shows severe agglomeration and loss of regular spherical shape (Figure 5e). This may be due to the fact that, at low ammonia concentrations, the precursors are unable to polymerize sufficiently on the surface of the SDBS micelles. Consequently, the yield is relatively low and the average particle size is small. In addition, the coefficient of variation is higher due to the insufficient amount of catalyst, which prevents uniform nucleation of individual microspheres. When the ammonia concentration is too high, an increased amount of NH_4^+ has a detrimental effect on the stability of the SDBS micelles. This affects the ability of the micelles to act as a template, preventing optimal growth of the microspheres and promoting their agglomeration.

Figure 6 shows the SEM images of RFS prepared with varying concentrations of SDBS, alongside the mean particle size, coefficient of variation, and yield of RFS with SDBS concentration. The resorcinol concentration was maintained at 0.5 mol/L, and the ammonia concentration was also 0.5 mol/L in this series of experiments. As can be observed in the SEM plots, the RFS prepared with different SDBS concentrations exhibited a narrow particle size distribution, good sphericity, and minimal variation between samples. Figure 6f illustrates that an increase in SDBS concentration from 5 to 30 g/L has a relatively minor impact on the particle size, coefficient of variation, and yield of RFS. This is due to the fact that the critical micelle concentration of SDBS is approximately 0.4 g/L, at which point SDBS is capable of forming micelles in solution. The SDBS concentrations employed in the experiments are all considerably in excess of its critical micelle concentration, and all are capable of fulfilling the requisite template function in the RFS synthesis process. This also indicates that an overhigh concentration of SDBS will not have an adverse effect on the nucleation and growth of RFS.

The data on precursor concentration and mean particle size from a selection of previously published papers were collated and subjected to comparison with the data presented in this study. The resulting data are displayed in Figure 7. The precursor concentration was used here as a measure of the yield. This is due to the fact that the majority of studies do not provide labeling for yield data, and in accordance with the findings of this study, the yield of RFS is approximately linearly related to the concentration of the precursor utilized during the standard polymerization of microspheres. From the figure, the RFS prepared in our study increased the range of the available precursor concentrations. Typically, the maximum

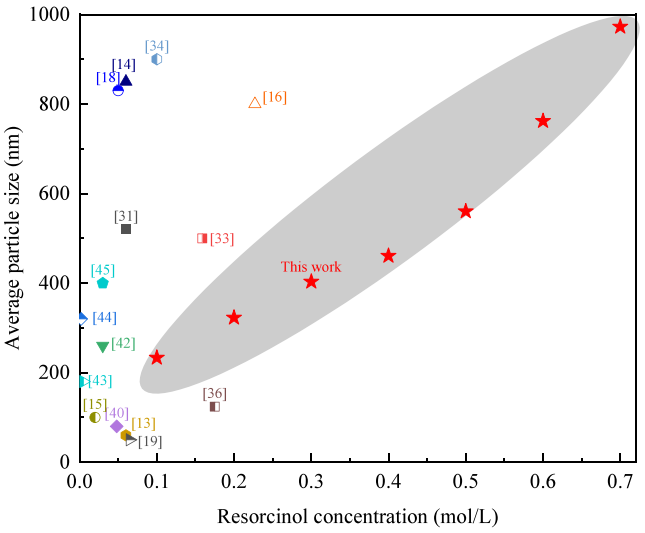

Figure 7. Comparison of RFS precursor concentration and average particle size in this work with other studies.

allowable precursor concentration for the preparation of RFS and CS is 0.3 mol/L. This study, however, has demonstrated the feasibility of increasing this concentration to 0.7 mol/L. The use of a higher precursor concentration, with an identical mean particle size of RFS, represents a significant advancement over the majority of the existing literature. This enables the preparation of RFS and CS with enhanced efficiency. The RFS prepared in our study also exhibits an advantage in the average particle size when the same precursor concentration is maintained. This suggests that the addition of SDBS effectively reduces the RFS particle size.

2.2. Carbonization of RFS. The RFS prepared at the resorcinol concentration of 0.5 mol/L (formaldehyde concentration: 1.0 mol/L, ammonia concentration: 0.5 mol/L, SDBS concentration: 10 g/L) was used as the sample for the subsequent carbonization experiments and was denoted as RFS-0.5R. The carbon microsphere samples obtained by carbonization of RFS-0.5R at 800, 900, and 1000 °C were denoted as CS-800, CS-900, and CS-1000, respectively.

Figure 8 shows the SEM images of CS prepared at different carbonization temperatures. From the figure, it can be seen that the RFS maintains a regular spherical morphology after the high-temperature carbonization process, and no agglomeration occurs between adjacent particles. The CS inherits the uniform spherical morphology of RFS well. The surface morphology is similar among the samples, indicating that the higher carbonization temperature does not affect the microscopic morphology of RFS significantly. The CS is further observed using TEM, as shown in Figure 8d, with a very regular spherical morphology and a smooth surface. And no graphite crystal structure is observed (Figure 8e and f), indicating that CS has amorphous properties.

The particle size of CS obtained from different carbonization temperatures was measured using ImageJ software, and the weights of RFS and CS before and after carbonization were weighed to calculate the weight loss rate at different carbonization temperatures. The results are shown in Table 1. The linear shrinkage of RFS increased from 20.8% to 23.8% as the carbonization temperature increased from 800 to 1000 °C, and the corresponding weight loss increased from 55.0% to 68.8%. The higher carbonization temperature leads to greater

https://doi.org/10.1021/acsomega.4c05590
ACS Omega 2024, 9, 43583−43592

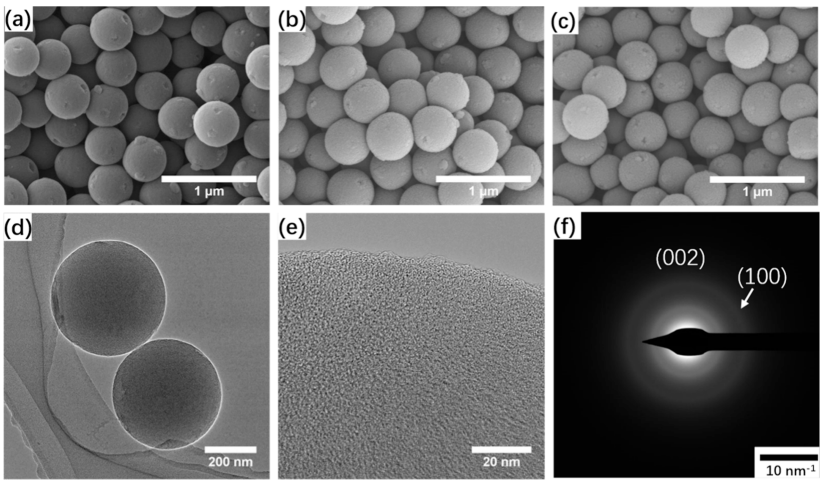

Figure 8. SEM images of (a) CS-800, (b) CS-900, and (c) CS-1000. (d, e) TEM images of CS-800 and (f) electron diffraction images of selected areas of CS-800.

Table 1. Average Particle Size, Linear Shrinkage, and Weight Loss of CS

carbonization temperature (°C)	average particle size (nm)	line shrinkage (%)	weight loss (%)
800	443.56	20.8	55.0
900	437.61	21.9	61.3
1000	427.05	23.8	68.8

shrinkage and weight loss, which is mainly due to more escape of small organic molecules from the RFS at higher temperatures. With a shrinkage of 20.8% and a weight loss of 55.0% at 800 °C carbonization, the maximum yield of CS could reach 41.9 g/L at a resorcinol concentration of 0.7 mol/L, and the particle size was only 770 nm.

2.3. Structure and Composition Characterization. Figure 9a shows the XRD patterns of RFS and CS. It can be

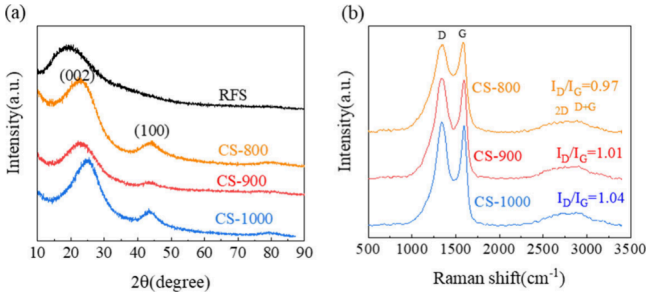

Figure 9. (a) XRD pattern and (b) Raman pattern of RFS and CS.

seen from the figure that the XRD pattern of RFS has a broad peak at 2θ of 20°, and the CS obtained by carbonization at different temperatures both have two broad peaks with 2θ near 23° and 43°, which belong to the (0 0 2) and (1 0 0) characteristic surfaces of amorphous carbon, respectively.[39] The broad peak package is typical of amorphous carbon, which is consistent with the results of the TEM. The peak intensity of CS-1000 at 2θ = 24° is significantly higher because higher carbonization temperatures are more likely to lead to CS graphitization. The Raman spectra of CS are shown in Figure 9b, both with relatively wide D and relatively narrow G bands. The D-band corresponds to the disordered structure or defective graphite structure of amorphous carbon, while the G-band indicates graphite carbon with sp^2 bonding structure. As the carbonization temperature increases, a gradual decrease in the half-peak width of the D and G bands can be observed, which is due to the increased graphitization in the CS at higher temperatures. The larger half-peak width of the D band than the G band indicates a higher proportion of disorder and defects in the CS.[34] The intensity ratio (I_D/I_G) of the D band to the G band can reflect the degree of graphitization of the carbon material. The I_D/I_G values for CS-800, CS-900, and CS-1000 have I_D/I_G values of 0.97, 1.01, and 1.04, respectively. This indicates that these samples are amorphous, which is consistent with the XRD results, and that the degree of graphitization of CS increases with increasing carbonization temperature. In addition, weak peaks belonging to the 2D band and G+D band can be observed at 2680 and 2920 cm^{-1}, which further indicate the low degree of graphitization of CS.

In order to better understand the surface properties of RFS, the FT-IR spectra of SDBS, RFS, and CS were tested, and the results are shown in Figure 10, where RFS-0S was the control sample without the addition of SDBS. From the figure, the FT-IR spectra of RFS-0.5R and RFS-0S have similar characteristic

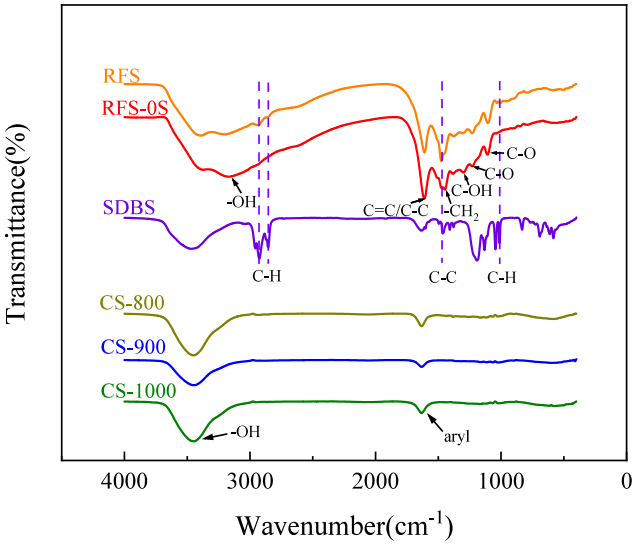

Figure 10. FT-IR spectra of the RFS, SDBS, and CS.

https://doi.org/10.1021/acsomega.4c05590
ACS Omega 2024, 9, 43583−43592

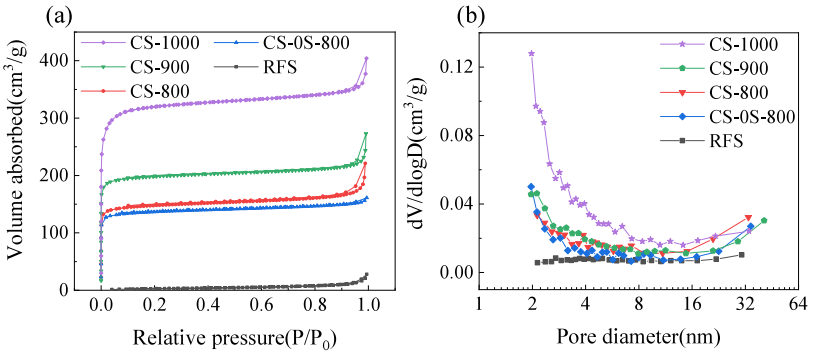

Figure 11. (a) Nitrogen adsorption−desorption curves and (b) pore size distribution curves of the RFS and CS.

peaks. The broad peak at 3170 cm^{-1} is the stretching vibration characteristic of the hydroxyl group (−OH). The peak at 1615 cm^{-1} corresponds to the stretching vibrations of C═C and C−C in the aromatic ring. The peak at 1450 cm^{-1} is the stretching vibration peak of $-CH_2$. The peak at 1295 cm^{-1} is related to the stretching vibration of the phenolic. The peaks at 1229 and 1104 cm^{-1} are the stretching vibrations of the intermolecular methylene ether C−O−C of resorcinol. By comparing the FT-IR spectra of RFS-0.5R, RFS-0S, and SDBS, it is obvious that RFS also contain characteristic peaks of SDBS, including 1008 cm^{-1} (bending vibration of aliphatic C−H), 1468 cm^{-1} (stretching vibration of C−C), and 2855 and 2925 cm^{-1} (stretching vibration of aliphatic C−H). This proves the presence of SDBS in RFS-0.5R samples, indicating the involvement of SDBS in the polymerization of RFS. After carbonization, the infrared spectra of CS at different temperatures are basically the same, mainly the vibrational peaks of hydroxyl and benzene rings, all of which lost most of their groups. This indicates that the carbonization reaction is basically completed when the carbonization temperature is 800 °C.

To investigate the changes in RFS pore structure after the carbonization process and the effect of carbonization temperature on the pore structure, RFS and CS were characterized by nitrogen adsorption analysis. The test results are shown in Figure 11 and Table 2. CS-0S-800 in the figure is the reference sample, which is the CS obtained without the addition of SDBS and carbonized at 800 °C.

Table 2. Pore Structure Parameters of the RFS and CS

sample	S_{BET} ($m^2.g^{-1}$)	S_{mes} ($m^2.g^{-1}$)	S_{mic} ($m^2.g^{-1}$)	V_{pore} ($cm^3.g^{-1}$)
RFS-0.5R	10.14	0	10.14	0.0455
CS-800	432.71	415.11	17.59	0.1751
CS-900	591.11	567.79	23.32	0.1376
CS-1000	979.10	937.94	41.16	0.1853
CS-0S-800	405.25	385.41	19.83	0.0543

Figure 11 shows that the adsorption of RFS-0.5R is very low, especially when the pressure is very low (P/P_0 is less than 0.1), and basically no adsorption occurs. With the gradual increase of P/P_0, the adsorption amount slowly increases, which is mainly due to the adsorption occurring in the pores accumulated between the RFS. The adsorption and desorption curves of CS obtained after carbonization exhibit a very significant microporous feature with the adsorption curve almost perpendicular to the transverse coordinate at P/P_0 close to 0. This is due to the presence of a large number of micropores resulting in the rapid increase of nitrogen adsorption. When P/P_0 continued to increase, the adsorption and desorption curves reached a smooth stage and CS-800 exhibited greater adsorption than CS-0S-800. This indicates that it has a larger specific surface area for gas adsorption. The adsorption continues to increase after P/P_0 increases to about 0.9, which is mainly due to the adsorption caused by the stacked pores between the CS. Eventually, the adsorption and desorption curves no longer continue to recombine and converge at the highest point, which implies a hysteresis loop between the adsorption and desorption curves. The adsorption−desorption curves of CS belong to the class I adsorption−desorption curves, indicating that the sample has a large number of micropores. Figure 11b shows the pore size distributions of the microspheres calculated according to the BJH model. It can be seen from the figure that RFS-0.5R without carbonization has almost no pores. A large number of pores are generated in the CS after carbonization at different temperatures, and the pore size is mainly concentrated in the range of 1−4 nm.

Table 2 shows that the specific surface area of RFS is very low, and there is no microporous pore at all. The specific surface area of RFS increases from 432.71 $m^2 \cdot g^{-1}$ to 979.10 $m^2 \cdot g^{-1}$ after carbonization from 800 to 1000 °C. The specific surface area of micropores increases significantly from 415.11 $m^2 \cdot g^{-1}$ to 937.94 $m^2 \cdot g^{-1}$. In contrast, the specific surface area of the mesopores shows only a modest change. This indicates that the increase in the specific surface area is mainly from the generation of micropores during the carbonization process. Furthermore, carbonization at 800 °C resulted in CS-800 with SDBS addition exhibiting a larger specific surface area and pore volume compared with CS-0S-800 without SDBS addition. This increase was primarily due to enhanced microporosity. This is the pore space left by the removal of SDBS micelles in the RFS during carbonization.

3. CONCLUSIONS

In conclusion, the effective preparation of CS on the submicrometer scale was accomplished by employing the anionic surfactant SDBS as a soft template. The simplicity of the raw materials and reaction conditions employed in this method ensures the safety, ease of operation, and low cost of the entire preparation process. Furthermore, the resulting CS exhibited a smooth surface, good monodispersity, and a high solution yield per unit volume. The concentration of the available carbon precursor can reach 0.7 mol/L, with an RFS yield of up to 93.2 g/L. After carbonization, the yield of CS at a diameter of 770 nm remains at 41.9 g/L, exhibiting excellent

https://doi.org/10.1021/acsomega.4c05590
ACS Omega 2024, 9, 43583−43592

monodispersity. Furthermore, the diameter of the resulting RFS can be readily adjusted within the range 200−1000 nm by modifying the concentrations of the precursors and catalysts. After carbonization under a nitrogen atmosphere at 800−1000 °C, the corresponding CS had uniform particle size and regular shape. A large number of micropores were generated within the CS, and the specific surface area increased with the increase of carbonization temperature, up to 937.94 $m^2 \cdot g^{-1}$. In addition, the results of the study showed that the incorporation of SDBS significantly increased the specific surface area of the CS.

4. EXPERIMENTAL SECTION

4.1. Material. Resorcinol ($C_6H_6O_2$, 99.5%) and formaldehyde solution (HCHO, 37% aqueous solution) were purchased from Shanghai Maclean Biochemical Technology Co. (China). Ammonia ($NH_3 \cdot H_2O$, 25% NH_3 aqueous solution) was purchased from Sinopharm Chemical Reagent Co. (China), and SDBS ($C_{18}H_{29}NaO_3S$, 95%) was purchased from Shanghai Aladdin Biochemical Technology Co. (China).

4.2. Preparation of RFS and Corresponding CS. First, SDBS (0.25 g, 10 g/L) and resorcinol (1.37 g, 0.5 mol/L) were dissolved in deionized water (25 mL) with constant stirring until the solids were completely dissolved. Then, formaldehyde solution (1.8 mL, 1 mol/L) and ammonia solution (0.934 mL, 0.5 mol/L) were added in turn. After being stirred for 5 min, the vessel was transferred to a water bath at 45 °C with constant stirring. After 12 h of reaction, the RFS were separated by centrifugation and washed three times with deionized water and anhydrous ethanol. The separated samples were dried in an oven at 80 °C. Among them, the properties of the resulting microspheres were regulated by varying the resorcinol concentration (0.1−0.7 mol/L), ammonia concentration (0.2−0.6 mol/L), and SDBS concentration (0−30 g/L).

Subsequently, the RFS were heated to specific temperatures (800, 900, and 1000 °C, respectively) under the protection of a nitrogen atmosphere at a heating rate of 5 °C/min and held for 1 h to carbonize the RFS to CS. For descriptive purposes, the carbon spheres were labeled with the temperature of the holding temperature and marked as CS-800, CS-900, and CS-1000, respectively.

4.3. Materials Characterization. The degree of graphitization of CS was analyzed using a German Bruker D8 Advance X-ray diffractometer and Netherlands Thermo DXR2 Raman spectrometer. The surface morphology of the samples was observed using a Czech Tescan mira4 scanning electron microscope and a Netherlands Themis Z transmission electron microscope, and the average particle size and coefficient variation of RFS and CS were measured and analyzed using ImageJ software. The specific surface area and pore size distribution of the samples were analyzed using an American Autosorb iQ specific surface area and pore size distribution analyzer. The sample weight loss temperature intervals and weight loss rates were characterized using a Swiss Mettler TGA/DSC 3+ thermogravimetric analyzer.

AUTHOR INFORMATION

Corresponding Authors

Junzong Feng − *Science and Technology on Advanced Ceramic Fibers and Composites Laboratory, College of Aerospace Science and Engineering, National University of Defense Technology, Changsha 410073, People's Republic of China*; orcid.org/0000-0001-6844-8950; Email: junzongfeng@nudt.edu.cn

Jian Feng − *Science and Technology on Advanced Ceramic Fibers and Composites Laboratory, College of Aerospace Science and Engineering, National University of Defense Technology, Changsha 410073, People's Republic of China*; Email: fengj@nudt.edu.cn

Authors

Jian Shao − *Science and Technology on Advanced Ceramic Fibers and Composites Laboratory, College of Aerospace Science and Engineering, National University of Defense Technology, Changsha 410073, People's Republic of China*

Yonggang Jiang − *Science and Technology on Advanced Ceramic Fibers and Composites Laboratory, College of Aerospace Science and Engineering, National University of Defense Technology, Changsha 410073, People's Republic of China*

Liangjun Li − *Science and Technology on Advanced Ceramic Fibers and Composites Laboratory, College of Aerospace Science and Engineering, National University of Defense Technology, Changsha 410073, People's Republic of China*; orcid.org/0000-0002-6581-5484

Yijie Hu − *Science and Technology on Advanced Ceramic Fibers and Composites Laboratory, College of Aerospace Science and Engineering, National University of Defense Technology, Changsha 410073, People's Republic of China*

Complete contact information is available at: https://pubs.acs.org/10.1021/acsomega.4c05590

Notes

The authors declare no competing financial interest.

ACKNOWLEDGMENTS

This work was supported by the Hunan Provincial Natural Science Foundation of China (No. 2023JJ30632) and Key R&D Program of Hunan Province (No. 2022GK2027).

REFERENCES

(1) Qiu, P.; Ma, B.; Hung, C.; Li, W.; Zhao, D. Spherical Mesoporous Materials from Single to Multilevel Architectures. *Acc. Chem. Res.* **2019**, *52* (10), 2928−2938.

(2) Huo, Y.; Xiu, S.; Meng, L.; Quan, B. Solvothermal synthesis and applications of micro/nano carbons: A review. *Chemical Engineering Journal* **2023**, *451* (40), 138572.

(3) Wang, G.; Qin, J.; Zhao, Y.; Wei, J. Nanoporous carbon spheres derived from metal-phenolic coordination polymers for supercapacitor and biosensor. *J. Colloid Interface Sci.* **2019**, *544*, 241−248.

(4) Feng, J.; Cai, R.; Magliocca, E.; Luo, H.; Higgins, L.; Romario, G. L. F.; Liang, X.; Pedersen, A.; Xu, Z.; Guo, Z.; Periasamy, A.; Brett, D.; Miller, T. S.; Haigh, S. J.; Mishra, B.; Titirici, M. M. Iron, Nitrogen Co-Doped Carbon Spheres as Low Cost, Scalable Electrocatalysts for the Oxygen Reduction Reaction. *Adv. Funct. Mater.* **2021**, *31* (46), No. 2102974.

(5) Ren, G.; Chen, S.; Zhang, J.; Zhang, N.; Jiao, C.; Qiu, H.; Liu, C.; Wang, H. N-doped porous carbon spheres as metal-free electrocatalyst for oxygen reduction reaction. *Journal of Materials Chemistry A* **2021**, *9* (9), 5751−5758.

(6) Mashindi, V.; Mente, P.; Mpofu, N.; Phaahlamohlaka, T. N.; Makgae, O.; Kirkland, A. I.; Forbes, R.; Ozoemena, K. I.; Levecque, P. B.; Coville, N. J. Platinum supported on pristine and nitrogen-doped bowl-like broken hollow carbon spheres as oxygen reduction reaction catalysts. *J. Appl. Electrochem.* **2021**, *51* (7), 991−1008.

https://doi.org/10.1021/acsomega.4c05590
ACS Omega 2024, 9, 43583−43592

(7) Yu, X.; Yi, J.; Zhang, R.; Wang, F.; Liu, L. Hollow carbon spheres and their noble metal-free hybrids in catalysis. *Frontiers of Chemical Science and Engineering* **2021**, *15* (6), 1380−1407.
(8) Tian, H.; Wang, T.; Zhang, F.; Zhao, S.; Wan, S.; He, F.; Wang, G. Tunable porous carbon spheres for high-performance rechargeable batteries. *J. Mater. Chem. A* **2018**, *6* (27), 12816−12841.
(9) Zong, L.; Fan, K.; Wu, W.; Cui, L.; Zhang, L.; Johannessen, B.; Qi, D.; Yin, H.; Wang, Y.; Liu, P.; Wang, L.; Zhao, H. Anchoring Single Copper Atoms to Microporous Carbon Spheres as High-Performance Electrocatalyst for Oxygen Reduction Reaction. *Adv. Funct. Mater.* **2021**, *31* (41), No. 2104864.
(10) Zhou, Y.; Yu, Y.; Ma, D.; Foucher, A. C.; Xiong, L.; Zhang, J.; Stach, E. A.; Yue, Q.; Kang, Y. Atomic Fe Dispersed Hierarchical Mesoporous Fe−N−C Nanostructures for an Efficient Oxygen Reduction Reaction. *ACS Catal.* **2021**, *11* (1), 74−81.
(11) Wang, H.; Yang, D.; Liu, S.; Yin, S.; Yu, H.; Xu, Y.; Li, X.; Wang, Z.; Wang, L. Cage-bell structured Pt@N-doped hollow carbon sphere for oxygen reduction electrocatalysis. *Chemical Engineering Journal* **2021**, *409*, No. 128101.
(12) Zhang, J.; Zhang, J.; He, F.; Chen, Y.; Zhu, J.; Wang, D.; Mu, S.; Yang, H. Y. Defect and Doping Co-Engineered Non-Metal Nanocarbon ORR Electrocatalyst. *Nano-Micro Letters* **2021**, *13*,65.
(13) Ghimire, P. P.; Dassanayake, A. C.; Wickramaratne, N. P.; Jaroniec, M. Polyvinyl pyrrolidone-assisted synthesis of size-tunable polymer spheres at elevated temperature and their conversion to nitrogen-containing carbon spheres. *J. Colloid Interface Sci.* **2019**, *549* (3), 162−170.
(14) Wang, X.; Zhou, J.; Xing, W.; Liu, B.; Zhang, J.; Lin, H.; Cui, H.; Zhuo, S. Resorcinol-formaldehyde resin-based porous carbon spheres with high CO_2 capture capacities. *Journal of Energy Chemistry* **2017**, *26* (5), 1007−1013.
(15) Du, J.; Liu, L.; Yu, Y.; Zhang, Y.; Lv, H.; Chen, A. N-doped ordered mesoporous carbon spheres derived by confined pyrolysis for high supercapacitor performance. *Journal of Materials Science & Technology* **2019**, *35* (10), 2178−2186.
(16) Liu, M.; Liu, L.; Yu, Y.; Lv, H.; Chen, A.; Hou, S. Synthesis of nitrogen-doped carbon spheres using the modified Stöber method for supercapacitors. *Frontiers of Materials Science* **2019**, *13* (2), 156−164.
(17) Vix-Guterl, C.; Frackowiak, E.; Jurewicz, K.; Friebe, M.; Parmentier, J.; Béguin, F. Electrochemical energy storage in ordered porous carbon materials. *Carbon* **2005**, *43* (6), 1293−1302.
(18) Du, X.; Yang, H.; Zhang, Y.; Hu, Q.; Li, S.; He, W. Synthesis of size-controlled carbon microspheres from resorcinol/formaldehyde for high electrochemical performance. *New Carbon Materials* **2021**, *36* (3), 616−624.
(19) Tsai, C.; Tai, H.; Su, C.; Chiang, L.; Li, Y. Activated Microporous Carbon Nanospheres for Use in Supercapacitors. *ACS Applied Nano Materials* **2020**, *3* (10), 10380−10388.
(20) Zhang, C.; Li, J.; Li, C.; Chen, W.; Guo, C. Surface and interface engineering of hollow carbon sphere-based electrocatalysts for the oxygen reduction reaction. *Journal of Materials Chemistry A* **2021**, *9* (46), 25706.
(21) Wang, S.; Chen, L.; Liu, X.; Long, L.; Liu, H.; Liu, C.; Dong, S.; Jia, J. Fe/N-doped hollow porous carbon spheres for oxygen reduction reaction. *Nanotechnology* **2020**, *31* (12), 125404−125404.
(22) Gong, Y.; Xie, L.; Li, H.; Wang, Y. Sustainable and scalable production of monodisperse and highly uniform colloidal carbonaceous spheres using sodium polyacrylate as the dispersant. *Chem. Commun.* **2014**, *50* (84), 12633−12636.
(23) Acharyulu, N. P. S.; Fakruddin Babavali, S. K.; Srinivasu, C. Nano structural transition metal oxide hollow spheres and carbon nano spherical structures by hydrothermal method and their characterization. *Materials Today: Proceedings* **2020**, *27*, 1455−1459.
(24) Gong, Y.; Xie, L.; Chen, C.; Liu, J.; Antonietti, M.; Wang, Y. Bottom-up hydrothermal carbonization for the precise engineering of carbon materials. *Prog. Mater. Sci.* **2023**, *132*, 101048−101105.
(25) Inada, M.; Enomoto, N.; Hojo, J.; Hayashi, K. Structural analysis and capacitive properties of carbon spheres prepared by hydrothermal carbonization. *Advanced Powder Technology* **2017**, *28* (3), 884−889.
(26) Maetz, A.; Delmotte, L.; Moussa, G.; Dentzer, J.; Knopf, S.; Ghimbeu, C. M. Facile and sustainable synthesis of nitrogen-doped polymer and carbon porous spheres. *Green Chem.* **2017**, *19* (9), 2266−2274.
(27) Tian, H.; Liang, J.; Liu, J. Nanoengineering Carbon Spheres as Nanoreactors for Sustainable Energy Applications. *Adv. Mater.* **2019**, *31* (50), 20−25.
(28) Zhao, J.; Gilani, M. R. H. S.; Liu, Z.; Luque, R.; Xu, G. Facile surfactant-free synthesis of polybenzoxazine-based polymer and nitrogen-doped carbon nanospheres. *Polymer chemistry* **2018**, *9* (33), 4324−4331.
(29) Wen, J.; Zhao, D.; Lu, Y.; Huang, J.; Li, Y.; Zhang, H.; Li, A. Simultaneous desulfurization and denitrogenation of model fuels by polyethylene glycol-modified resorcinol/formaldehyde resin-derived carbon spheres. *Korean Journal of Chemical Engineering* **2019**, *36* (7), 1131−1139.
(30) Sibera, D.; Narkiewicz, U.; Kapica, J.; Serafin, J.; Michalkiewicz, B.; Wróbel, R. J.; Morawski, A. W. Preparation and characterisation of carbon spheres for carbon dioxide capture. *Journal of Porous Materials* **2019**, *26* (1), 19−27.
(31) Liu, J.; Qiao, S. Z.; Liu, H.; Chen, J.; Orpe, A.; Zhao, D.; Lu, G. Q. M. Extension of The Stöber Method to the Preparation of Monodisperse Resorcinol-Formaldehyde Resin Polymer and Carbon Spheres. *Angew. Chem., Int. Ed.* **2011**, *50* (26), 5947−5951.
(32) Zheng, Y.; Chen, S.; Zhang, K. A. I.; Guan, J.; Yu, X.; Peng, W.; Song, H.; Zhu, J.; Xu, J.; Fan, X.; Zhang, C.; Liu, T. Template-free construction of hollow mesoporous carbon spheres from a covalent triazine framework for enhanced oxygen electroreduction. *J. Colloid Interface Sci.* **2022**, *608*, 3168−3177.
(33) Fan, C.; Ou, M.; Wei, P.; Xu, J.; Sun, S.; Liu, Y.; Xu, Y.; Fang, C.; Li, Q.; Han, J. Hard carbon spheres prepared by a modified Stöber method as anode material for high-performance potassium-ion batteries. *RSC Adv.* **2021**, *11* (24), 14883−14890.
(34) Zhao, X.; Zhang, M.; Sun, X.; Li, X.; Li, J. Comprehensive understanding of the formation process on monodisperse resorcinol-formaldehyde polymer and carbon spheres and their use as substrates for surface-enhanced Raman spectroscopy. *Appl. Surf. Sci.* **2020**, *506* (30), 144591.
(35) Wei, J.; Wang, G.; Chen, F.; Bai, M.; Liang, Y.; Wang, H.; Zhao, D.; Zhao, Y. Sol-Gel Synthesis of Metal-Phenolic Coordination Spheres and Their Derived Carbon Composites. *Angew. Chem., Int. Ed.* **2018**, *57* (31), 9838−9843.
(36) Li, X.; Song, Y.; You, L.; Gao, L.; Liu, Y.; Chen, W.; Mao, L. Synthesis of Highly Uniform N-Doped Porous Carbon Spheres Derived from Their Phenolic-Resin-Based Analogues for High Performance Supercapacitors. *Ind. Eng. Chem. Res.* **2019**, *58* (8), 2933−2944.
(37) Yu, Q.; Guan, D.; Zhuang, Z.; Li, J.; Shi, C.; Luo, W.; Zhou, L.; Zhao, D.; Mai, L. Mass Production of Monodisperse Carbon Microspheres with Size-Dependent Supercapacitor Performance via Aqueous Self-Catalyzed Polymerization. *ChemPlusChem.* **2017**, *82* (6), 872−878.
(38) Yang, T.; Liu, J.; Zhou, R.; Chen, Z.; Xu, H.; Qiao, S. Z.; Monteiro, M. J. N-doped mesoporous carbon spheres as the oxygen reduction reaction catalysts. *Journal of Materials Chemistry A* **2014**, *2* (42), 18139−18146.
(39) Wang, J.; Liu, H.; Sun, H.; Hua, W.; Wang, H.; Liu, X.; Wei, B. One-pot synthesis of nitrogen-doped ordered mesoporous carbon spheres for high-rate and long-cycle life supercapacitors. *Carbon* **2018**, *127*, 85−92.
(40) Hu, L.; Qian, Z.; Gao, W.; Wang, X.; Tian, Y. Nanoengineering of uniform and monodisperse mesoporous carbon nanospheres mediated by long hydrophilic chains of triblock copolymers. *J. Mater. Sci.* **2020**, *55* (5), 2052−2067.
(41) Wang, A.; Zhu, Q.; Xing, Z. A functionalized chitosan wrinkled hollow sphere containing calcium ions: Efficient adsorption of sodium

https://doi.org/10.1021/acsomega.4c05590
ACS Omega 2024, 9, 43583−43592

dodecylbenzenesulfonate (SDBS) from aqueous solutions. *J. Colloid Interface Sci.* **2019**, *555*, 203−213.
(42) Liu, M.; Yu, Y.; Liu, B.; Liu, L.; Lv, H.; Chen, A. PVP-assisted synthesis of nitrogen-doped hollow carbon spheres for supercapacitors. *J. Alloys Compd.* **2018**, *768*, 42−48.
(43) Wang, Q. G.; He, L.; Zhao, L. Y.; Liu, R. S.; Zhang, W. P.; Lu, A. H. Surface Charge-Driven Nanoengineering of Monodisperse Carbon Nanospheres with Tunable Surface Roughness. *Adv. Funct. Mater.* **2020**, *30* (6), 117−125.
(44) Yu, X.; Li, W.; Hu, Y.; Ye, C.; Lu, A. Sculpturing solid polymer spheres into internal gridded hollow carbon spheres under controlled pyrolysis micro-environment. *Nano Research* **2021**, *14* (5), 1565−1573.
(45) Du, J.; Zhang, Y.; Wu, H.; Hou, S.; Chen, A. N-doped hollow mesoporous carbon spheres by improved dissolution-capture for supercapacitors. *Carbon* **2020**, *156*, 523−528.

https://doi.org/10.1021/acsomega.4c05590
ACS Omega 2024, 9, 43583−43592